

Computing differential operators of the particle velocity in moving particle clouds using tessellations

Thibault Oujia^{1,*}, Keigo Matsuda², and Kai Schneider¹

¹ *Institut de Mathématiques de Marseille,*

Aix-Marseille Université, CNRS, France and

² *Japan Agency for Marine-Earth Science and Technology (JAMSTEC), Japan*

(Dated: December 8, 2022)

Abstract

We propose finite-time measures to compute the divergence, the curl and the velocity gradient tensor of the point particle velocity for two- and three-dimensional moving particle clouds. To this end, tessellation of the particle positions is applied to associate a volume to each particle. Considering then two subsequent time instants, the dynamics of the volume can be assessed. Determining the volume change of tessellation cells yields the divergence of the particle velocity and the rotation of the cells evaluates its curl. Thus the helicity of particle velocity can be likewise computed and swirling motion of particle clouds can be quantified. We propose a modified version of Voronoi tessellation which overcomes some drawbacks of the classical Voronoi tessellation. First we assess the numerical accuracy for randomly distributed particles. We find strong Pearson correlation between the divergence computed with the modified version, and the analytic value which confirms the validity of the method. Moreover, the modified Voronoi-based method converges with first order in space and time in two and three dimensions for randomly distributed particles, which is not the case for the classical Voronoi tessellation. Furthermore, we consider for advecting particles, random velocity fields with imposed power-law energy spectra, motivated by turbulence. We determine the number of particles necessary to guarantee a given precision. Finally, applications to fluid particles advected in three-dimensional fully developed isotropic turbulence show the utility of the approach for real world applications to quantify self-organization in particle clouds and their vortical or even swirling motion.

* thibault.oujia@univ-amu.fr

I. INTRODUCTION

The general context of this work are flows of point particle clouds evolving in time where inertial particles are transported by an underlying flow velocity, the so-called the carrier phase. Such configurations are typically encountered in multiphase flows, especially when the carrier phase velocity is turbulent. Particle laden turbulent flows occur in many natural and engineering systems, for instance droplets in clouds in the atmosphere, sand storms in the desert or spray combustion with liquid fuels. Observations show that inertial particles in turbulent flow exhibit a non-uniform spatial distribution, i.e., preferential concentration, resulting in the emergence of void and cluster regions [15, 16]. Understanding of the complex dynamics of these fundamental cluster and void formation processes is a prerequisite for sound modeling and important for numerous applications.

The divergence of the particle velocity, a scalar-valued signed quantity, allows to quantify the divergence and convergence of particles corresponding to positive and negative divergence values, respectively. The divergence of the particle velocity is contained in the source term in the particle density balance equation. The curl of the particle velocity, a vector valued quantity, yields insight about the local rotation rate of particles, i.e., the particle vorticity and thus quantifies vortical motion of particle clouds. Likewise important to characterize swirling motion is the flow helicity which quantifies the alignment of the particle velocity and the particle vorticity. The ultimate goal is to access the particle velocity gradient tensor, and to consider its trace, the symmetric and anti-symmetric parts.

However, it is not straight forward to determine quantities such as divergence and curl of the particle velocity due to its discrete nature, i.e., the velocity is only defined at particle positions. One approach to deal with the problem for instance in homogeneous periodic flow would be to determine the particle velocity from the particle flux. The particle flux is given by the convolution of the particle density with the particle velocity and in principle we could compute the particle velocity by solving a deconvolution problem. However, the particle positions are not given on a uniform grid. Hence the Fast Fourier Transform (FFT) cannot be used, which makes this problem very expensive and even unfeasible for a large number of particles. Interpolating the particle velocity data on a regular grid, using e.g. Fourier, or other interpolation methods would be likewise possible. Then the derivative of the particle velocity could be computed by deriving the interpolating function. However

interpolating values given on random particle positions has its own difficulties. For solving PDEs and also for computing differential operators different meshfree methods have been developed, some review detailing the major directions, i.e. smooth particle hydrodynamics and moving least-squares, is given in Huerta *et al.* [5].

Voronoi and Delaunay tessellations allow the definition of natural neighbors for arbitrary unstructured grids. Voronoi tessellation has been applied to analyze data from different origins, e.g. astrophysics, biology, particle-laden turbulence [2, 4, 11]. The volume of Voronoi cells yields the local density of a set of points. Using Voronoi tessellation, statistics are not affected by an arbitrary choice, like the bin size, for defining for instance the particle density. A mimetic method to compute divergence and curl operators on unstructured grids using Voronoi and Delaunay tessellations has been developed in Vabishchevich [17], by refining a velocity gradient on the Voronoi and Delaunay cells. This approach allows to define the different operators in two and three space dimensions. However, using this method the truncation error was shown to be in general of order $\mathcal{O}(1)$, except for regular grids. Sozer *et al.* [14] assessed the accuracy of gradient reconstruction methods for cell-centered data on unstructured meshes. A Green–Gauss method is used for gradient calculation with different interpolation stencils. It is shown that several gradient operators have first order accuracy, regardless of the cell shape. However, there is not one gradient operator that provides the lowest error for all cell configurations.

For computing derivatives we need at least two point information. Here we combine tessellations and a Lagrangian approach to compute efficiently the divergence, curl and velocity gradient tensor of the particle velocity by considering the time change of a modified Voronoi tessellation of the particle cloud. In Oujia *et al.* [12] we proposed a finite–time measure to quantify the divergence, by computing the time change of the volume change rate of the Voronoi volume and presented some preliminary validation. In the present study, we aim to analyze the method in detail, propose some modifications to improve the existing method and perform numerical analysis on the accuracy of the method to compute the divergence. Then we generalize this approach to compute the curl and the velocity gradient tensor of the particle velocity using using volume change of tessellation cell. Helicity of the particle velocity can also be computed and thus we can quantify swirling motion of particle clouds. Detailed assessment of the methods is conducted for particles distributed randomly and transported by a given velocity field in order to compute the error between the exact

value and the value obtained with the method. Then we consider synthetic turbulent velocity fields in order to have a lower bound of the accuracy of the method for data coming from turbulence. Finally, we advect particles with turbulent velocity fields computed by direct numerical simulation and test the method for a practically relevant case.

The outline of the manuscript is as follows. In section II we summarize the principle of Voronoi tessellation and explain the mathematical foundation of the proposed approach to quantify the divergence, curl and velocity gradient tensor of particle velocity using volume change. In section III we provide information on the reliability and convergence orders of our method. In section IV we apply the methods to fluid particles in turbulence. Finally, conclusions are drawn in section V.

II. DIFFERENTIAL OPERATORS BASED ON VOLUME CHANGE

In this section we explain the mathematical foundation of our method to define finite-time measures to quantify spatial differential operators. First, Voronoi and Delaunay tessellations of particle clouds are described, including some mathematical background. Then, we present how to calculate the divergence from the volume change over time and adapt the method to enable the calculation of the curl and the velocity gradient tensor of the particle velocity. Finally, we convert this Lagrangian method into an Eulerian method and estimate the truncation error.

A. Voronoi and Delaunay tessellations

The Voronoi tessellation [18] decomposes the space seeded with particles into cells; a Voronoi cell \mathcal{C}_i generated by the particle p_i represents the region of space closer to the particle p_i than to all the others. A Voronoi cell can be interpreted as the influence volume of a particle. The volumes of the Voronoi cells are inversely proportional to the particle density. For instance, we can use the size of the cells to identify clusters of particles. Indeed, a set of small cells is the sign of a local concentration of particles and a set of large cells indicates a low density region. A quality of the Voronoi tessellation is that the tessellation is constructed without introducing an arbitrary length scale. The Delaunay tessellation [3] of a set of particles p is a tessellation such that no particles are inside the

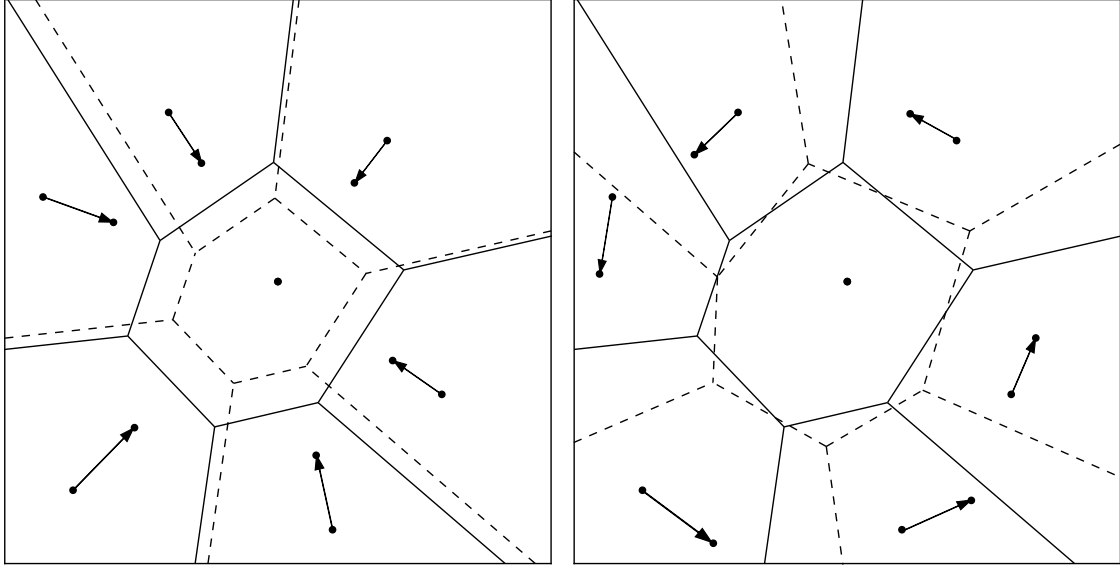


Figure 1. Example of the motion of a two-dimensional Voronoi tessellation at two subsequent time instants for a compression (left) and a rotation (right). The solid line corresponds to the time step t^k and the dashed line to t^{k+1} . The arrows indicate the particle velocity.

circumscribed circle of one of any cells. The Delaunay tessellation of a set of particles p is the dual graph of the Voronoi tessellation. The vertices of the Voronoi tessellation are the centers of the circumscribed circles of the cells of the Delaunay tessellation. Another way to define a cell corresponding to a particle, instead of using the circumcenter of the Delaunay cell as done for the Voronoi tessellation, is to use the center of gravity of the Delaunay cell to define the vertices of the cell. In the following, the tessellation using the center of gravity of the Delaunay cell is called modified Voronoi tessellation. We will see later that this construction yields more accurate results. To compute the Voronoi and the Delaunay tessellation, we use the Quickhull algorithm provided by the Qhull library in python [1], which has a computational complexity of $\mathcal{O}(N \log(N))$, where N denotes the number of particles.

Figure 1 illustrates a possible evolution of a two-dimensional Voronoi cell over time. On the left figure we can observe a compression of the Voronoi cell, while on the right we can see a rotation of the cell. We can discern that in the case of compression the volume of the Voronoi cell is reduced and that in the case of rotation the cell is likewise rotated. In this study, we focus on two and three dimensions, but all results can be applied to higher dimensions.

B. Divergence of particle velocity using volume change

In this subsection, we first recall the method proposed in Oujia *et al.* [12] to define the finite time–discrete divergence of the particle velocity based on the time change of the Voronoi volume. Motivated by stability concerns this method will be here also extended using modified Voronoi volumes.

The particles are transported by a velocity field. Thus we have access to the particle velocity at the discrete particle position. Particles in a flow domain $\Omega \subset \mathbb{R}^d$, $d = 2, 3$, satisfy the conservation equation,

$$D_t n = \partial_t n + \mathbf{v} \cdot \nabla n = -n \nabla \cdot \mathbf{v}, \quad (1)$$

also proposed in IJzermans *et al.* [6], where $n > 0$ is the particle number density, \mathbf{v} is the particle velocity, and $D_t n$ is the Lagrangian derivative of n . We use the notation $\partial_t \equiv \partial/\partial t$ and $\nabla = (\partial/\partial x, \partial/\partial y, \partial/\partial z)$. Dividing by the particle density n and considering the particle density at two time instants t^k and $t^{k+1} = t^k + \Delta t$, the discrete divergence $\mathcal{D} \equiv \nabla \cdot \mathbf{v}$ can be defined using the particle density n as,

$$\mathcal{D} \equiv -\frac{1}{n} D_t n = -\frac{1}{2} \left(\frac{1}{n^{k+1}} + \frac{1}{n^k} \right) \frac{n^{k+1} - n^k}{\Delta t} + \mathcal{O}(\Delta t) \quad (2)$$

To obtain the particle distribution at time t^{k+1} particles are advected by the particle velocity, e.g., using the explicit Euler method, $\mathbf{x}_p^{k+1} = \mathbf{x}_p^k + \Delta t \mathbf{v}_p^k$ where \mathbf{x}_p and \mathbf{v}_p are the position and velocity of the p -th particle, respectively.

The equation originally proposed in Oujia *et al.* [12] is

$$\mathcal{D} \equiv -\frac{2}{n^{k+1} + n^k} \frac{n^{k+1} - n^k}{\Delta t} + \mathcal{O}(\Delta t)$$

but the weakness of this formula is that for a fixed value of n^k and Δt

$$\lim_{n^{k+1} \rightarrow 0} \mathcal{D} = \frac{2}{\Delta t}$$

while the value should tend to infinity. Another temporal approximation of the particle density n is possible using the logarithmic derivative,

$$\mathcal{D} \equiv -\ln \left(\left(\frac{n^{k+1}}{n^k} \right)^{1/\Delta t} \right) + \mathcal{O}(\Delta t)$$

However, we do not use this formula either, because for large density variation the divergence does not vary by the same order of magnitude. This is not the case in equation (2).

The local number density over a Voronoi cell n_p , a piecewise constant function, is defined as $n_p = V_p^{-1}$, with V_p being the volume of the cell. Similarly, the local number density can be defined also based on modified Voronoi cells, i.e., defined based on centers of gravity instead of circumcenters. Replacing the particle density n by this discrete value in equation (2), we obtain a finite-time discrete divergence of the particle velocity based on tessellation cells defined as,

$$\mathcal{D}(\mathbf{v}_p) = \frac{1}{2\Delta t} \left(\frac{1}{V_p^{k+1}} + \frac{1}{V_p^k} \right) (V_p^{k+1} - V_p^k) \quad (3)$$

which is analyzed and used in the following.

C. Rotation of particle velocity using volume change

The curl of the particle velocity can be defined by computing the circulation of the velocity field of particles over a cell. We can express the curl of a vector-valued function \mathbf{v} as the divergence of a function \mathbf{v}^\perp where \mathbf{v}^\perp is \mathbf{v} projected onto the orthogonal plane of the direction of the curl through the origin and rotated in a direction by $\pi/2$ with respect to the direction of the curl,

$$\nabla \times \mathbf{v} = \begin{pmatrix} \frac{\partial v_z}{\partial y} - \frac{\partial v_y}{\partial z} \\ \frac{\partial v_x}{\partial z} - \frac{\partial v_z}{\partial x} \\ \frac{\partial v_y}{\partial x} - \frac{\partial v_x}{\partial y} \end{pmatrix} = \begin{pmatrix} 0 & -\frac{\partial}{\partial z} & \frac{\partial}{\partial y} \\ \frac{\partial}{\partial z} & 0 & -\frac{\partial}{\partial x} \\ -\frac{\partial}{\partial y} & \frac{\partial}{\partial x} & 0 \end{pmatrix} \begin{pmatrix} v_x \\ v_y \\ v_z \end{pmatrix} = - \begin{pmatrix} \nabla \cdot \mathbf{v}_x^\perp \\ \nabla \cdot \mathbf{v}_y^\perp \\ \nabla \cdot \mathbf{v}_z^\perp \end{pmatrix} \quad (4)$$

with $\mathbf{v}_x^\perp = \mathbf{L}_x \mathbf{v}$, $\mathbf{v}_y^\perp = \mathbf{L}_y \mathbf{v}$ and $\mathbf{v}_z^\perp = \mathbf{L}_z \mathbf{v}$ where

$$\mathbf{L}_x = \begin{pmatrix} 0 & 0 & 0 \\ 0 & 0 & -1 \\ 0 & 1 & 0 \end{pmatrix}, \quad \mathbf{L}_y = \begin{pmatrix} 0 & 0 & 1 \\ 0 & 0 & 0 \\ -1 & 0 & 0 \end{pmatrix} \quad \text{and} \quad \mathbf{L}_z = \begin{pmatrix} 0 & -1 & 0 \\ 1 & 0 & 0 \\ 0 & 0 & 0 \end{pmatrix}.$$

Note that $\{\mathbf{L}_x, \mathbf{L}_y, \mathbf{L}_z\}$ is the most common basis of the Lie algebra of the rotation group $SO(3)$ [7]. By reusing the discrete divergence \mathcal{D} defined in subsection II B, the discrete curl \mathcal{C} of the particle velocity can be computed at particle positions.

Using equation (4) the discrete curl is defined as

$$\mathbf{C}(\mathbf{v}_p) = \begin{pmatrix} \mathcal{D}(-\mathbf{v}_{p,x}^\perp) \\ \mathcal{D}(-\mathbf{v}_{p,y}^\perp) \\ \mathcal{D}(-\mathbf{v}_{p,z}^\perp) \end{pmatrix}. \quad (5)$$

In two dimensions, the curl reduces to a pseudo-scalar $\mathcal{C}(\mathbf{v}_p) = \mathcal{D}(-\mathbf{v}_p^\perp)$ where \mathbf{v}_p^\perp is the particle velocity \mathbf{v}_p , rotated $\pi/2$ in counter-clockwise direction in the two-dimensional plane.

D. Velocity gradient tensor of the particle velocity using volume change

More generally, the gradient tensor, i.e., the different partial derivatives of a vector-valued function can be computed as the divergence of each of its components projected onto the different axes of the vector space, as detailed below. In three dimensions, the velocity gradient tensor is defined and can be rewritten as,

$$\nabla \mathbf{v} = \begin{pmatrix} \frac{\partial v_x}{\partial x} & \frac{\partial v_x}{\partial y} & \frac{\partial v_x}{\partial z} \\ \frac{\partial v_y}{\partial x} & \frac{\partial v_y}{\partial y} & \frac{\partial v_y}{\partial z} \\ \frac{\partial v_z}{\partial x} & \frac{\partial v_z}{\partial y} & \frac{\partial v_z}{\partial z} \end{pmatrix} = \begin{pmatrix} \nabla \cdot (v_x \mathbf{e}_x) & \nabla \cdot (v_x \mathbf{e}_y) & \nabla \cdot (v_x \mathbf{e}_z) \\ \nabla \cdot (v_y \mathbf{e}_x) & \nabla \cdot (v_y \mathbf{e}_y) & \nabla \cdot (v_y \mathbf{e}_z) \\ \nabla \cdot (v_z \mathbf{e}_x) & \nabla \cdot (v_z \mathbf{e}_y) & \nabla \cdot (v_z \mathbf{e}_z) \end{pmatrix} \quad (6)$$

with

$$\mathbf{e}_x = \begin{pmatrix} 1 & 0 & 0 \end{pmatrix}^T; \mathbf{e}_y = \begin{pmatrix} 0 & 1 & 0 \end{pmatrix}^T; \mathbf{e}_z = \begin{pmatrix} 0 & 0 & 1 \end{pmatrix}^T$$

Using the volume change technique to compute the discrete divergence of components of the function \mathbf{v}_p projected on the different space axes, we can define the discrete gradient \mathcal{G} of the velocity \mathbf{v}_p at particle positions as

$$\mathcal{G}(\mathbf{v}_p) = \begin{pmatrix} \mathcal{D}(v_x \mathbf{e}_x) & \mathcal{D}(v_x \mathbf{e}_y) & \mathcal{D}(v_x \mathbf{e}_z) \\ \mathcal{D}(v_y \mathbf{e}_x) & \mathcal{D}(v_y \mathbf{e}_y) & \mathcal{D}(v_y \mathbf{e}_z) \\ \mathcal{D}(v_z \mathbf{e}_x) & \mathcal{D}(v_z \mathbf{e}_y) & \mathcal{D}(v_z \mathbf{e}_z) \end{pmatrix} \quad (7)$$

In a similar way, we can compute the velocity gradient tensor in two dimensions.

E. Conversion into an Eulerian formulation and truncation error

Here, we focus on the three-dimensional case, similar results can be derived in two dimensions. We consider four points p_0 , p_1 , p_2 , and p_3 . Here p_0 is considered to be the center

particle, and p_1 , p_2 , and p_3 are considered to be vertices of a tessellation cell. The position and velocity vectors of p_j ($j = 0, 1, 2$, and 3) are \mathbf{x}_j and \mathbf{v}_j , respectively. We define the relative position vector $\mathbf{r}_j = \mathbf{x}_j - \mathbf{x}_0$ and the relative velocity vector $\mathbf{w}_j = \mathbf{v}_j - \mathbf{v}_0$ for $j = 1, 2$, and 3 . The volume V of the parallelepiped generated by the points p_0 , p_1 , p_2 , and p_3 is given by $V = (\mathbf{r}_1 \times \mathbf{r}_2) \cdot \mathbf{r}_3$. Note that the volume of the tetrahedron is $1/6$ of the one of the parallelepiped. The volume change of the tetrahedron is then given by

$$\begin{aligned} \frac{dV}{dt} &= \lim_{\Delta t \rightarrow 0} \frac{V(t + \Delta t) - V(t)}{\Delta t} \\ &= \lim_{\Delta t \rightarrow 0} \frac{1}{\Delta t} [\{(\mathbf{r}_1 + \mathbf{w}_1 \Delta t) \times (\mathbf{r}_2 + \mathbf{w}_2 \Delta t)\} \cdot (\mathbf{r}_3 + \mathbf{w}_3 \Delta t) - (\mathbf{r}_1 \times \mathbf{r}_2) \cdot \mathbf{r}_3] \\ &= \lim_{\Delta t \rightarrow 0} \frac{1}{\Delta t} [(\mathbf{r}_2 \times \mathbf{r}_3) \cdot \mathbf{w}_1 \Delta t + (\mathbf{r}_3 \times \mathbf{r}_1) \cdot \mathbf{w}_2 \Delta t + (\mathbf{r}_1 \times \mathbf{r}_2) \cdot \mathbf{w}_3 \Delta t + \mathcal{O}(\Delta t^2)] \\ &= [(\mathbf{r}_2 \times \mathbf{r}_3) \cdot \mathbf{w}_1 + (\mathbf{r}_3 \times \mathbf{r}_1) \cdot \mathbf{w}_2 + (\mathbf{r}_1 \times \mathbf{r}_2) \cdot \mathbf{w}_3] \end{aligned} \quad (8)$$

Thus, assuming that the terms of $\mathcal{O}(\Delta t)$ are negligibly small, we have

$$\mathcal{D} = \frac{1}{V} \frac{dV}{dt} = \frac{1}{V} [\mathbf{w}_1 \cdot (\mathbf{r}_2 \times \mathbf{r}_3) + \mathbf{w}_2 \cdot (\mathbf{r}_3 \times \mathbf{r}_1) + \mathbf{w}_3 \cdot (\mathbf{r}_1 \times \mathbf{r}_2)] \quad (9)$$

Note that in 2D, \mathbf{r}_3 is replaced by the unit normal vector $\mathbf{n} = \mathbf{r}_1 \times \mathbf{r}_2 / |\mathbf{r}_1 \times \mathbf{r}_2|$, and \mathbf{w}_3 is replaced by $\mathbf{0}$.

When we use the unit normal vectors $\hat{\mathbf{r}}_j = \mathbf{r}_j / |\mathbf{r}_j|$ for $j = 1, 2$, and 3 , the divergence is given by

$$\mathcal{D} = \frac{\hat{\mathbf{r}}_2 \times \hat{\mathbf{r}}_3}{\hat{V}} \cdot \frac{\mathbf{w}_1}{|\mathbf{r}_1|} + \frac{\hat{\mathbf{r}}_3 \times \hat{\mathbf{r}}_1}{\hat{V}} \cdot \frac{\mathbf{w}_2}{|\mathbf{r}_2|} + \frac{\hat{\mathbf{r}}_1 \times \hat{\mathbf{r}}_2}{\hat{V}} \cdot \frac{\mathbf{w}_3}{|\mathbf{r}_3|}, \quad (10)$$

where $\hat{V} = V / (|\mathbf{r}_1| |\mathbf{r}_2| |\mathbf{r}_3|)$.

We consider the coordinate transformation in Cartesian coordinates of (x_1, x_2, x_3) into (ξ_1, ξ_2, ξ_3) , in which a vector $\mathbf{x} = x_1 \mathbf{e}_1 + x_2 \mathbf{e}_2 + x_3 \mathbf{e}_3$ is transformed into $\mathbf{x} = \xi_1 \mathbf{r}_1 + \xi_2 \mathbf{r}_2 + \xi_3 \mathbf{r}_3$. The divergence of \mathbf{v} in the transformed coordinates is then given by

$$\nabla \cdot \mathbf{v} = \mathbf{e}^j \frac{\partial}{\partial x_j} \cdot \mathbf{v} = \mathbf{e}^j \frac{\partial \xi_k}{\partial x_j} \frac{\partial}{\partial \xi_k} \cdot \mathbf{v} = \mathbf{r}^k \frac{\partial}{\partial \xi_k} \cdot \mathbf{v}, \quad (11)$$

where \mathbf{e}^j is the reciprocal basis of Cartesian coordinates, and \mathbf{r}^j is the reciprocal basis given by

$$\begin{aligned} \mathbf{r}^1 &= \frac{\mathbf{r}_2 \times \mathbf{r}_3}{(\mathbf{r}_2 \times \mathbf{r}_3) \cdot \mathbf{r}_1}, \\ \mathbf{r}^2 &= \frac{\mathbf{r}_3 \times \mathbf{r}_1}{(\mathbf{r}_3 \times \mathbf{r}_1) \cdot \mathbf{r}_2}, \\ \mathbf{r}^3 &= \frac{\mathbf{r}_1 \times \mathbf{r}_2}{(\mathbf{r}_1 \times \mathbf{r}_2) \cdot \mathbf{r}_3}. \end{aligned}$$

Note that $(\mathbf{r}_2 \times \mathbf{r}_3) \cdot \mathbf{r}_1 = (\mathbf{r}_3 \times \mathbf{r}_1) \cdot \mathbf{r}_2 = (\mathbf{r}_1 \times \mathbf{r}_2) \cdot \mathbf{r}_3 = V$.

Now we consider the Taylor expansion of a function $f(\mathbf{x})$ given by,

$$f(\mathbf{x} + \mathbf{r}) = \lim_{n \rightarrow +\infty} \sum_{k=0}^n \frac{1}{k!} (\mathbf{r} \cdot \nabla)^k f(\mathbf{x}) \quad (12)$$

Applying the Taylor expansion to the velocity field up to third order we obtain

$$\frac{\mathbf{v}(\mathbf{x} + \mathbf{r}) - \mathbf{v}(\mathbf{x})}{|\mathbf{r}|} = (\hat{\mathbf{r}} \cdot \nabla) \mathbf{v}(\mathbf{x}) + \frac{|\mathbf{r}|}{2!} (\hat{\mathbf{r}} \cdot \nabla)^2 \mathbf{v}(\mathbf{x}) + \frac{|\mathbf{r}|^2}{3!} (\hat{\mathbf{r}} \cdot \nabla)^3 \mathbf{v}(\mathbf{x}) + \mathcal{O}(|\mathbf{r}|^3) \quad (13)$$

By applying equation (13) to $\mathbf{w}_j/|\mathbf{r}_j|$ ($j = 1, 2$, and 3) in equation (10), we obtain

$$\begin{aligned} \mathcal{D} &= \frac{\hat{\mathbf{r}}_2 \times \hat{\mathbf{r}}_3}{\hat{V}} \cdot (\hat{\mathbf{r}}_1 \cdot \nabla) \mathbf{v}(\mathbf{x}_0) + \frac{\hat{\mathbf{r}}_3 \times \hat{\mathbf{r}}_1}{\hat{V}} \cdot (\hat{\mathbf{r}}_2 \cdot \nabla) \mathbf{v}(\mathbf{x}_0) + \frac{\hat{\mathbf{r}}_1 \times \hat{\mathbf{r}}_2}{\hat{V}} \cdot (\hat{\mathbf{r}}_3 \cdot \nabla) \mathbf{v}(\mathbf{x}_0) \\ &+ \frac{\hat{\mathbf{r}}_2 \times \hat{\mathbf{r}}_3}{\hat{V}} \cdot \frac{|\mathbf{r}_1|}{2!} (\hat{\mathbf{r}}_1 \cdot \nabla)^2 \mathbf{v}(\mathbf{x}_0) + \frac{\hat{\mathbf{r}}_3 \times \hat{\mathbf{r}}_1}{\hat{V}} \cdot \frac{|\mathbf{r}_2|}{2!} (\hat{\mathbf{r}}_2 \cdot \nabla)^2 \mathbf{v}(\mathbf{x}_0) + \frac{\hat{\mathbf{r}}_1 \times \hat{\mathbf{r}}_2}{\hat{V}} \cdot \frac{|\mathbf{r}_3|}{2!} (\hat{\mathbf{r}}_3 \cdot \nabla)^2 \mathbf{v}(\mathbf{x}_0) \\ &+ \mathcal{O}(|\mathbf{r}|^2) \end{aligned} \quad (14)$$

Here, we have $(\hat{\mathbf{r}}_j \cdot \nabla) \mathbf{v} = \left(\hat{\mathbf{r}}_j \cdot \mathbf{r}^k \frac{\partial}{\partial \xi_k} \right) \mathbf{v} = \frac{1}{|\mathbf{r}_j|} \left(\delta_j^k \frac{\partial}{\partial \xi_k} \right) \mathbf{v} = \frac{1}{|\mathbf{r}_j|} \frac{\partial \mathbf{v}}{\partial \xi_j}$ for $j = 1, 2$, and 3 . Thus, the first three terms on the right-hand side correspond to the velocity divergence $\nabla \cdot \mathbf{v}$ at the position $\mathbf{x} = \mathbf{x}_0$, and we get

$$\begin{aligned} \mathcal{D} &= (\nabla \cdot \mathbf{v})_{\mathbf{x}=\mathbf{x}_0} \\ &+ \frac{\hat{\mathbf{r}}_2 \times \hat{\mathbf{r}}_3}{\hat{V}} \cdot \frac{|\mathbf{r}_1|}{2!} (\hat{\mathbf{r}}_1 \cdot \nabla)^2 \mathbf{v}(\mathbf{x}_0) + \frac{\hat{\mathbf{r}}_3 \times \hat{\mathbf{r}}_1}{\hat{V}} \cdot \frac{|\mathbf{r}_2|}{2!} (\hat{\mathbf{r}}_2 \cdot \nabla)^2 \mathbf{v}(\mathbf{x}_0) + \frac{\hat{\mathbf{r}}_1 \times \hat{\mathbf{r}}_2}{\hat{V}} \cdot \frac{|\mathbf{r}_3|}{2!} (\hat{\mathbf{r}}_3 \cdot \nabla)^2 \mathbf{v}(\mathbf{x}_0) \\ &+ \mathcal{O}(|\mathbf{r}|^2) \end{aligned} \quad (15)$$

In the present tessellation-based method, the volume change is calculated for the total volume of the tetrahedrons neighboring p_0

$$\mathcal{D}_p = \frac{\sum_m \mathcal{D}_{\text{tetra},m} V_{\text{tetra},m}}{\sum_m V_{\text{tetra},m}} \quad (16)$$

with $\mathcal{D}_{\text{tetra},m}$ being the divergence computed using equation (9) at the m -th tetrahedron position neighboring p_0 .

$$\begin{aligned} \mathcal{D}_p \sum_m V_{\text{tetra},m} &= (\nabla \cdot \mathbf{v})_{\mathbf{x}=\mathbf{x}_0} \sum_m V_{\text{tetra},m} \\ &+ \frac{1}{12} \sum_m (\mathbf{r}_{m,2} \times \mathbf{r}_{m,3}) \cdot |\mathbf{r}_{m,1}| (\mathbf{r}_{m,1} \cdot \nabla)^2 \mathbf{v}(\mathbf{x}_0) \\ &+ \frac{1}{12} \sum_m (\mathbf{r}_{m,3} \times \mathbf{r}_{m,1}) \cdot |\mathbf{r}_{m,2}| (\mathbf{r}_{m,2} \cdot \nabla)^2 \mathbf{v}(\mathbf{x}_0) \\ &+ \frac{1}{12} \sum_m (\mathbf{r}_{m,1} \times \mathbf{r}_{m,2}) \cdot |\mathbf{r}_{m,3}| (\mathbf{r}_{m,3} \cdot \nabla)^2 \mathbf{v}(\mathbf{x}_0) + \mathcal{O}(V|\mathbf{r}|^2) \end{aligned} \quad (17)$$

We can generalize equation (17) for arbitrary weights. We consider

$$\mathcal{D}_p = \sum_m W_m \mathcal{D}_{\text{tetra},m}, \quad (18)$$

where the weights satisfy, $\sum_m W_m = 1$,

$$\begin{aligned} \mathcal{D}_p &= (\nabla \cdot \mathbf{v})_{\mathbf{x}=\mathbf{x}_0} \\ &+ \sum_m W_m \mathbf{r}_m^1 \cdot |\mathbf{r}_{m,1}| (\mathbf{r}_{m,1} \cdot \nabla)^2 \mathbf{v}(\mathbf{x}_0) \\ &+ \sum_m W_m \mathbf{r}_m^2 \cdot |\mathbf{r}_{m,2}| (\mathbf{r}_{m,2} \cdot \nabla)^2 \mathbf{v}(\mathbf{x}_0) \\ &+ \sum_m W_m \mathbf{r}_m^3 \cdot |\mathbf{r}_{m,3}| (\mathbf{r}_{m,3} \cdot \nabla)^2 \mathbf{v}(\mathbf{x}_0) + \mathcal{O}(|\mathbf{r}|^2) \end{aligned} \quad (19)$$

The derivative of \mathbf{v} is dependent on the tessellation. We observed that in the case of a Cartesian grid or a hexagonal tiling, the first order terms cancel out which allows to obtain a second order convergence.

III. NUMERICAL VALIDATION OF THE METHOD

In this section we illustrate the weakness of the Voronoi tessellation for the derivative computation and show that the modified Voronoi tessellation allows to overcome this drawback. Then the reliability of the method and the convergence rate in space and time of the modified Voronoi-based method for computing a derivative and a sum of derivatives, for a given velocity field are assessed. Moreover, a study of the accuracy as a function of the wavenumber and as a function of the number of particles for a random velocity fields with imposed power-law energy spectra encountered in turbulence is carried out. In the different cases, particles are advected using the explicit Euler scheme.

A. Drawback of Voronoi tessellation

The reliability of the method of the discrete Voronoi-based divergence for randomly distributed particles has been checked in the Appendix A of Oujia *et al.* [12]. We observed a strong correlation between the exact divergence and the Voronoi-based divergence and that the error is most important in strain dominated regions. The Pearson correlation is a measure of linear correlation between two data sets. In the case where this coefficient

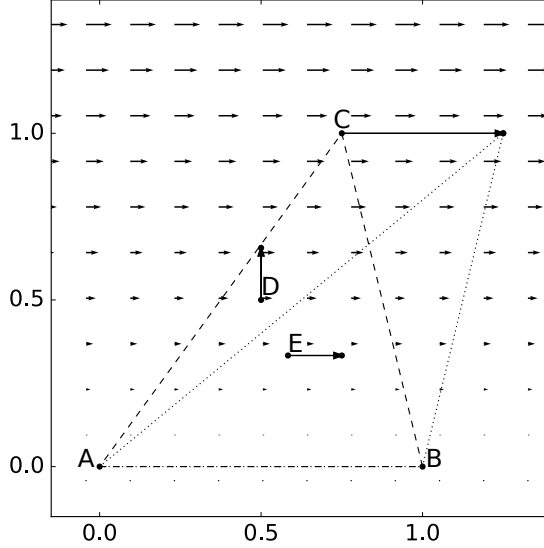


Figure 2. Motion of a triangle formed by particles A , B and C , the circumcenter D and the center of gravity E for a linear shear flow. The arrows indicate the particle motion.

does not tend to 1 no convergence in space or time is achieved. We also observed that when the number of particles increases, the Pearson correlation increases but then saturates at a value of $r = 0.936$. The Pearson correlation does not tend to $r = 1$ due to a geometrical error. The reason is that the deformation of a Voronoi cell is not exactly the same as the deformation of a fluid volume in the continuous setting. One of the geometrical effects can be explained by a leverage effect induced by the motion of circumcenters, as explained with the following example. We consider a linear shear flow, $\mathbf{u}(x, y) = (y, 0)$ advecting a triangle of three particles A , B and C with $A = (0, 0)$, $B = (1, 0)$ and $C = (1, 1)$, represented in figure 2. Here D is the center of the circumscribed circle. We observe that when the particles are advected by the velocity \mathbf{u} , the circumcenter D is shifted upwards, whereas it should shift towards the same direction as the other points. The motion of the point D can therefore result in an increase in the volume of a cell even in the case of zero divergence. Moreover, the divergence being defined as the ratio of the volume variation with the volume, if we reduce the size of the cell, the error remains unchanged and persists regardless of the scale. On the opposite, if we define E as the center of gravity of the triangle, we can see that its motion is similar to that of the shear. Using the modified Voronoi tessellation for the same velocity field as in the Appendix A of Oujia *et al.* [12], we obtain that the Pearson correlation tends to $r = 1$. For this reason, in the following, we will focus only on the

modified Voronoi tessellation.

B. Computation of a spatial derivative

In the following we verify numerically the validity of the method for the computation of a derivative using the modified Voronoi-based method in two and three dimensions. To this end, we consider randomly distributed particles in a 2π -periodic domain Ω advected by a given velocity field. The derivative is computed using the variation of the modified Voronoi volume. In two dimensions, we compare the modified Voronoi-based method with the Weighted Tri-Linear Face Interpolation (WTLI) method from Sozer *et al.* [14].

1. Two dimensions

In two dimensions, in order to check the reliability of the method in terms of convergence in space and time, we consider the following velocity field,

$$\mathbf{u}(x, y) = \begin{pmatrix} \sin(x) \cos(y) \\ 0 \end{pmatrix} \quad x, y \in \Omega \quad (20)$$

whose partial derivative in x -direction is, $\partial u_x / \partial x = \cos(x) \cos(y)$. Figure 3 shows the L^2 error of $\partial u_x / \partial x$ for two-dimensional randomly distributed particles as a function of Δt for a fixed number of particles N (a) and as a function of N for fixed Δt (b). We observe first order convergence in time and order one-half for N , i.e., first order in space as N denotes the total number of particles in 2D. The plateau is due to the coupling between Δt and N .

Now we compare these results with an existing gradient computation method described in Sozer *et al.* [14] which uses the Green-Gauss Gradient Method. The WTLI method is used for simplicity of implementation as well as the fact that the different presented methods (e.g., Weighted Least Squares Face Interpolation or Least Squares Gradient Method) give equivalent results. The gradient of \mathbf{u} in a closed area V is defined as

$$\nabla \mathbf{u} = \frac{1}{V} \sum_{e=1}^{N_{\text{edges}}} \bar{\mathbf{u}}_e \hat{\mathbf{n}}_e A_e$$

where N_{edges} is the number of edges of the cell formed by the tessellation, A_e is the length of the edge e , $\hat{\mathbf{n}}_e$ is the edge unit normal vector and $\bar{\mathbf{u}}_e$ is the average of \mathbf{u} over the edge e .

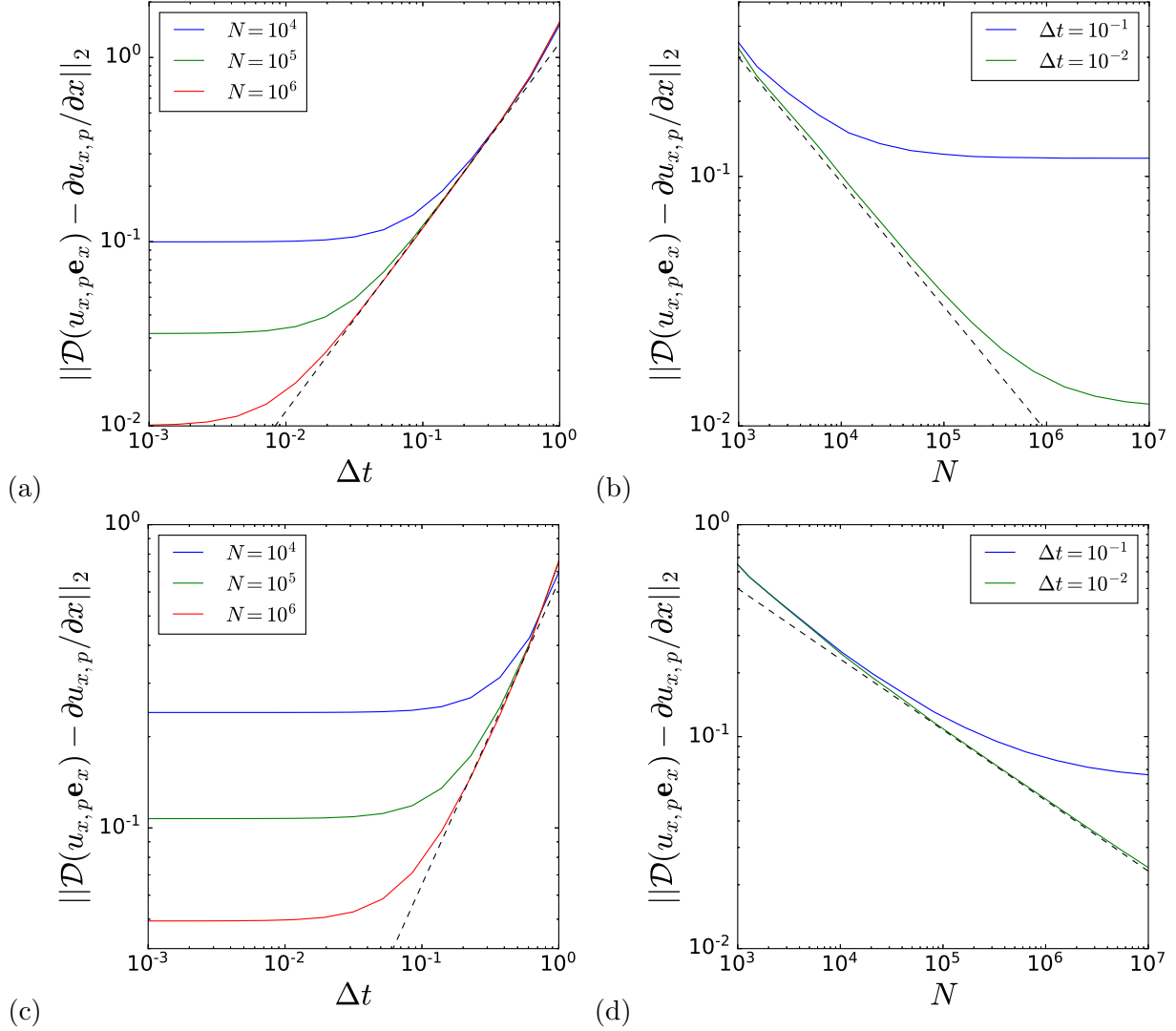


Figure 3. L^2 error of the gradient as function of Δt (a,c) and N (b,d) for two (a,b) and three dimensions (c,d) for randomly distributed particles using the modified Voronoi-based method. Dashed lines indicate slope 1 (a,c), $-1/2$ (b) and $-1/3$ (d).

Using the WTLI method, the value of $\bar{\mathbf{u}}_e$ is interpolated at the center of the edge e using the velocity of three adjacent particles p_i ($i = 1, 2$, and 3):

$$\bar{\mathbf{u}}_e = C_1 \mathbf{u}_1 + C_2 \mathbf{u}_2 + C_3 \mathbf{u}_3$$

where \mathbf{u}_i is the velocity of p_i and where the coefficients C_1 , C_2 and C_3 are obtained by

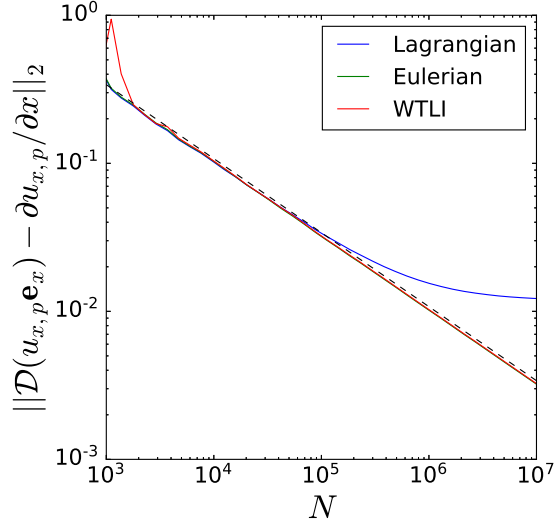


Figure 4. L^2 error of the gradient using Lagrangian and Eulerian modified Voronoi-based method and WTLI method computed for two-dimensional randomly distributed particles as function of N . Dashed line has slope $-1/2$.

solving

$$\begin{pmatrix} x_1 & x_2 & x_3 \\ y_1 & y_2 & y_3 \\ 1 & 1 & 1 \end{pmatrix} \begin{pmatrix} C_1 \\ C_2 \\ C_3 \end{pmatrix} = \begin{pmatrix} x_c \\ y_c \\ 1 \end{pmatrix}$$

where (x_c, y_c) is the center of the edge e and (x_i, y_i) is the position of the point p_i .

Figure 4 shows the L^2 error of $\partial u_x / \partial x$ using the Lagrangian ($\Delta t = 10^{-2}$) and Eulerian modified Voronoi-based method, i.e., computed respectively with equation (3) and (9), and the WTLI method computed for two-dimensional randomly distributed particles as function of N using the exact value of the particle velocity \mathbf{u} . We observe that the results for the different methods are similar. We find order one-half for N , i.e., first order in space, for the different methods and a saturation of the error for the Lagrangian method due to the coupling with Δt .

2. Three dimensions

In order to verify the reliability of the method in three dimensions in terms of convergence in space and time we consider the following velocity field,

$$\mathbf{u}(x, y, z) = \begin{pmatrix} \sin(x) \cos(y) \cos(z) \\ 0 \\ 0 \end{pmatrix} \quad x, y, z \in \Omega \quad (21)$$

whose partial derivative in x -direction is $\partial u_x / \partial x = \cos(x) \cos(y) \cos(z)$. Figure 3 shows the L^2 error of $\partial u_x / \partial x$ for three-dimensional randomly distributed particles as a function of Δt for a fixed number of particles N (c) and as a function of N for a fixed Δt (d). We can observe first order in time and an order one-third for N , yielding first order in space. Again the saturation of the error for large values of N and small Δt is due to the coupling between Δt and N .

So we can conclude that the method converges with a first order in time and in each space direction for randomly distributed particles.

C. Computation of the sum of derivatives

Now we verify numerically the validity of the method for the computation of a sum of derivatives required for the divergence or the curl of the particle velocity. Indeed, the method being initially designed for the computation of the divergence, gives us the ability to compute simultaneously the sum of derivatives of a function by rearranging the different components of the function. In this section we will compute the divergence and show that the method converges with the same order in space and time for the sum of partial derivatives.

1. Divergence in two dimensions

First we analyze the convergence of the discrete divergence operator in space and time in two dimensions. We consider the following velocity field,

$$\mathbf{u}(x, y) = \begin{pmatrix} \cos(x) \cos(y) \\ -\sin(x) \sin(y) \end{pmatrix} \quad x, y \in \Omega \quad (22)$$

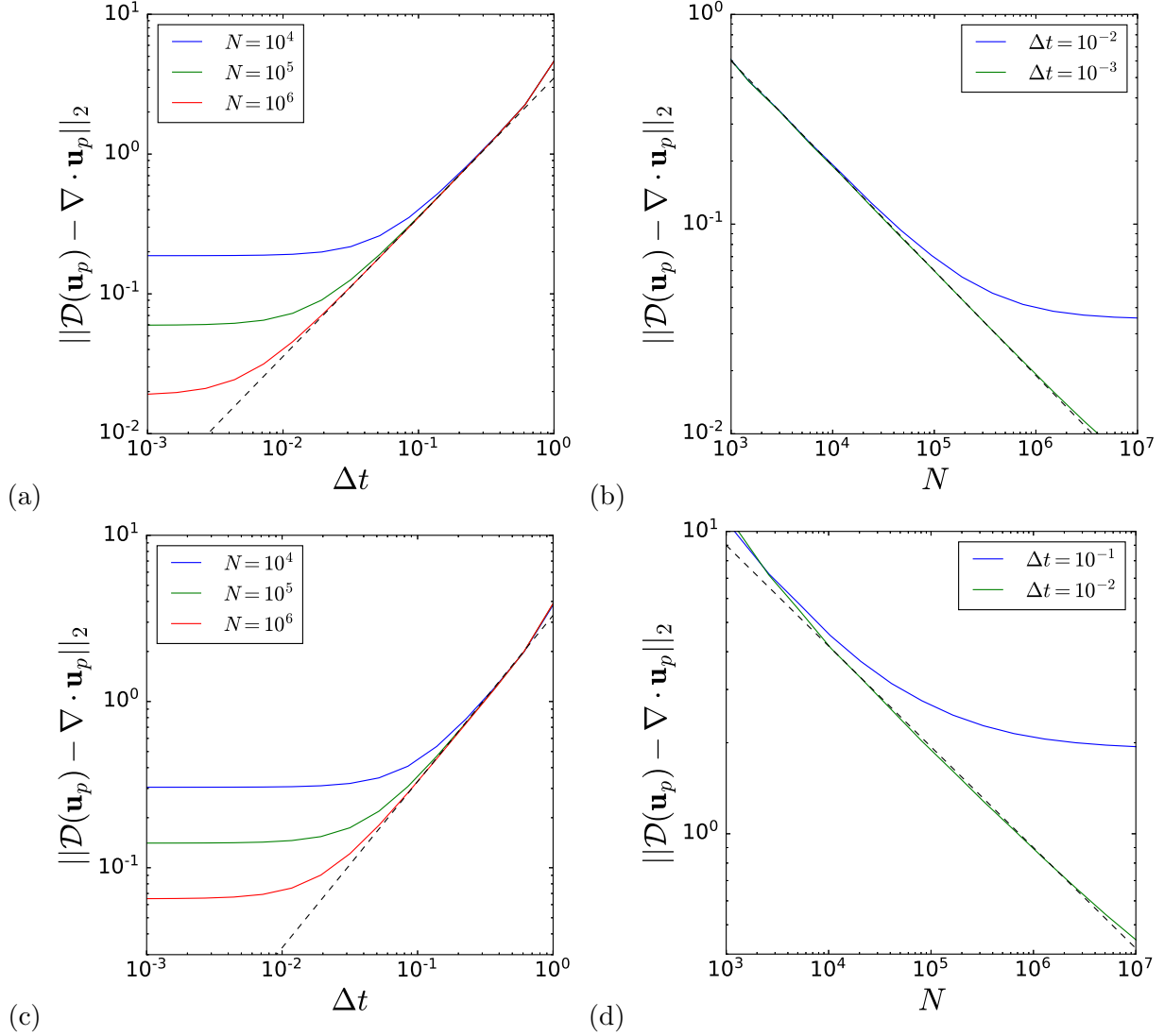


Figure 5. L^2 error of the divergence as a function of Δt (a,c) and N (b,d) for two (a,b) and three dimensions (c,d) for randomly distributed particles using the modified Voronoi-based method. Dashed lines indicate slopes 1 (a,c), $-1/2$ (b) and $-1/3$ (d).

whose divergence is $\nabla \cdot \mathbf{u}(x, y) = -2 \sin(x) \cos(y)$. Figure 5 shows the L^2 error $\|\mathcal{D}_p - \nabla \cdot \mathbf{u}_p\|_2$ as a function of Δt for a fixed number of particles N and as a function of N for fixed Δt . We can observe first order in time and order one-half for N , meaning first order in space. As expected, the results are comparable to those in figure 3(a,b).

2. Divergence in three dimensions

In three dimensions, we consider the velocity field

$$\mathbf{u}(x, y, z) = \begin{pmatrix} \sin(x) \cos(y) \cos(z) \\ \cos(x) \sin(y) \cos(z) \\ \cos(x) \cos(y) \sin(z), \end{pmatrix} \quad x, y, z \in \Omega \quad (23)$$

whose divergence is $\nabla \cdot \mathbf{u}(x, y, z) = 3 \cos(x) \cos(y) \cos(z)$, and verify the reliability of the method. Figure 5 shows a decay of the L^2 error with slope 1 for the error in time, and a slope of $-1/3$ for N , meaning first order in space for randomly distributed particles. As in two dimensions, the results are comparable to those of figure 3 (c,d), which confirms that the method allows to compute simultaneously the sum of derivatives and thus the divergence or curl with the same order of approximation.

D. Curl of synthetic turbulent velocity fields and required particle number

We consider synthetic turbulent velocity fields, i.e., random fields with a given correlation, for advecting randomly distributed particles. The energy spectrum satisfies a power law, with slopes typically observed in two- and three-dimensional turbulence. The question is then to assess how many particles are needed as function of the wavenumber to have a good correlation between the exact values and computed values using the tessellation-based method. In a first step we take $N = 100^d$ particles ($d = 2, 3$), compute the derivative of a sine wave with given wavenumber k in a 2π -periodic domain, $\mathbf{u}_k^{2D}(x, y) = (\sin(kx), 0)$ in two dimensions and $\mathbf{u}_k^{3D}(x, y, z) = (\sin(kx), 0, 0)$ in three dimensions for different $k \in [1 : 100]$. Then we calculate the Pearson correlation between the exact derivative value and the numerical one. Figure 6 (a) shows the Pearson correlation of a sine function as function of the normalized number on particles $N^{1/d}/k$, where $d = 2, 3$ is the dimension. As expected, the more particles we have per wavelength, the larger the Pearson correlation is. We can conclude that for a value close to $N^{1/d}/k = 10$ the Pearson correlation is $r = 0.99$ in two and three dimensions, which corresponds to a very strong correlation.

In the next step the goal is to apply the method to synthetic turbulence whose energy spectrum satisfies a power law behavior. In order to have a lower bound estimation of the accuracy of the method in the case of the computation of the vorticity, i.e. the curl of the

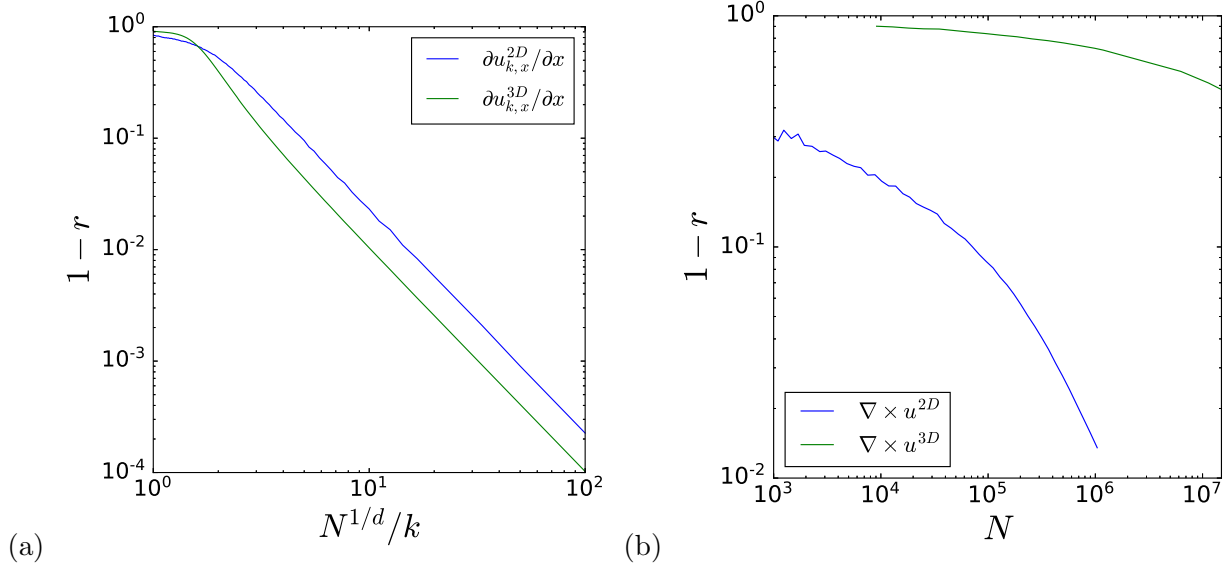


Figure 6. Pearson correlation r between the exact derivative values and computed values using the modified Voronoi-based derivative as function of the normalized number of particles $N^{1/d}$ ($d = 2, 3$) divided by the wavenumber k (left) in two and three dimensions. Pearson correlation between the exact curl values and computed values using the modified Voronoi-based curl as function the number of particles for velocity fields with imposed power-law energy spectra (right) in two and three dimensions.

velocity of a turbulent flow, we consider a realization of random functions \mathbf{u}^{2D} and \mathbf{u}^{3D} which are the sum of sines with a random phase defined as,

$$\mathbf{u}^{2D}(x, y) = \sum_{k=1}^{k_{\max}} E(k)^{1/2} \begin{pmatrix} \sin(kx + r_{k,0}) + \sin(ky + r_{k,1}) \\ \sin(kx + r_{k,2}) + \sin(ky + r_{k,3}) \end{pmatrix}$$

$$\mathbf{u}^{3D}(x, y, z) = \sum_{k=1}^{k_{\max}} E(k)^{1/2} \begin{pmatrix} \sin(kx + r_{k,0}) + \sin(ky + r_{k,1}) + \sin(kz + r_{k,2}) \\ \sin(kx + r_{k,3}) + \sin(ky + r_{k,4}) + \sin(kz + r_{k,5}) \\ \sin(kx + r_{k,6}) + \sin(ky + r_{k,7}) + \sin(kz + r_{k,8}) \end{pmatrix}$$

where $r_{k,j} \in [0, 2\pi[$ for $j = 0, \dots, 8$ are uniformly distributed random numbers, and $E(k) = k^{-3}$ in two dimensions and $k^{-5/3}$ in three dimensions. We take $k_{\max} = 256$ to be able to compare the results with a numerical simulation with a resolution of 512^d ($d = 2, 3$). Figure 6 (b) shows the Pearson correlation of $\nabla \times \mathbf{u}^{2D}$ and $\nabla \times \mathbf{u}^{3D}$. We observe that even if theoretically the high wavenumbers are poorly resolved as we can see in figure 6 (a), the fact that their coefficients are low does not prevent us to find a strong correlation of the Pearson

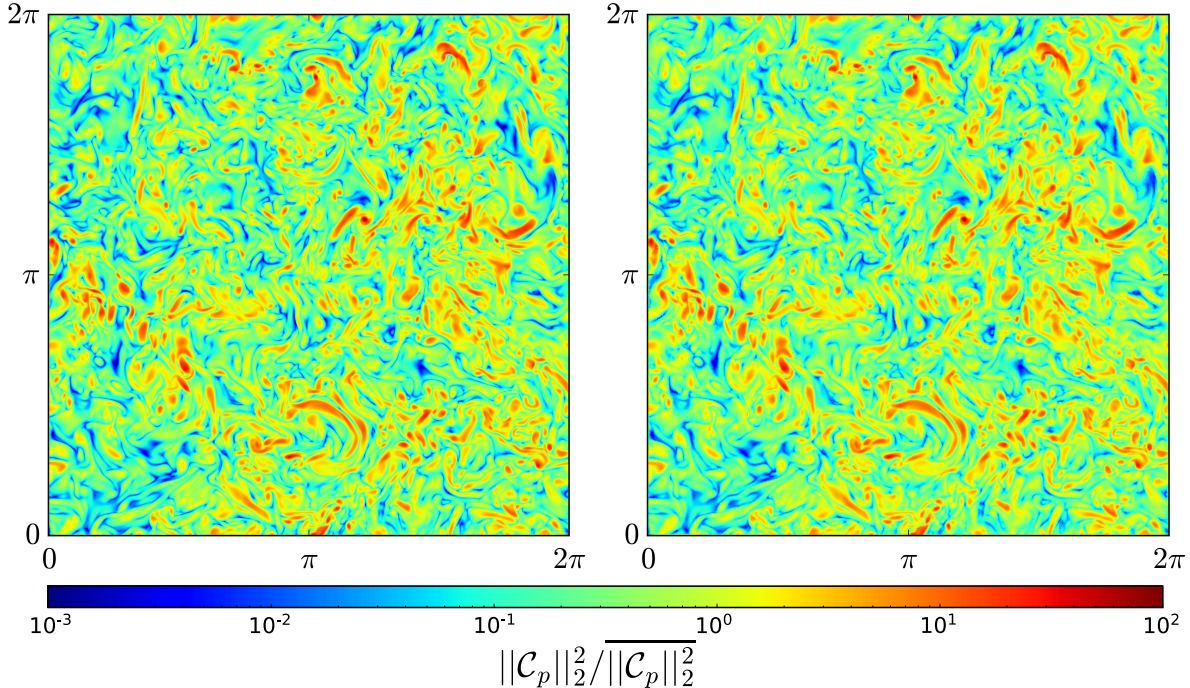


Figure 7. L^2 norm squared of the curl normalized by the mean value of the turbulent flow in a slice of $2\pi/512$ of the domain computed on an Eulerian grid (left) and with the modified Voronoi-based curl (right) at time $t = 21T_0$.

coefficient.

IV. APPLICATION TO TURBULENCE

In this section, we test our method for data from Direct Numerical Simulation (DNS) of particle-laden homogeneous isotropic turbulence, detailed in Matsuda *et al.* [8, 9]. The incompressible Navier–Stokes equations are solved in a 2π -periodic cube with a fourth-order finite-difference scheme. A large scale forcing is applied to obtain a statistically stationary flow. Uniformly distributed discrete particles are then injected into the fully developed flow and the fluid velocities at the particle positions are sampled. State of the art high resolution DNS with $N_g^3 = 512^3$ grid points is performed for the Taylor-microscale Reynolds number $Re_\lambda = 204$. The number of fluid particles N_p is 1.5×10^7 for the first data set and 1.07×10^9 for the second data set.

Figure 7 shows the L^2 norm squared of the curl normalized by the mean value computed on an Eulerian grid (left) and for fluid particles with the modified Voronoi-based curl (right)

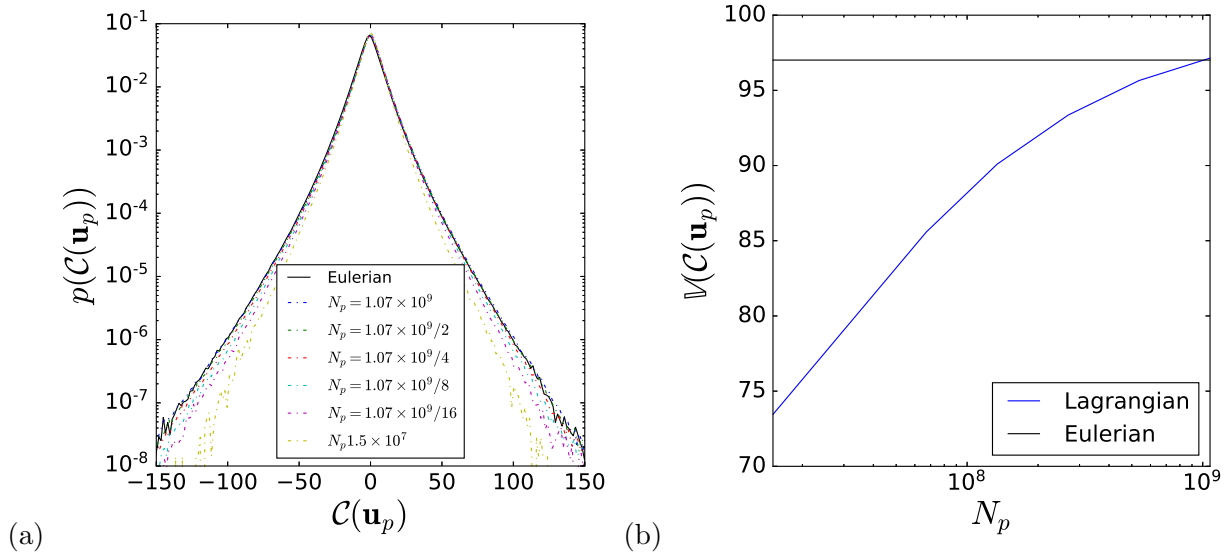


Figure 8. PDFs of fluid vorticity (left) and variance (right) of the fluid vorticity for different values of N_p computed for fluid particles and on Eulerian grid.

using the second data set. We can observe a perfect agreement between the two methods. To obtain figure 7 (right) the average value of the curl at particle position was computed on a grid of size 512^2 . This result gives some confidence and good expectations applying the modified Voronoi-based curl to real flow data either obtained by DNS or by particle tracking velocimetry (PTV) of experiments.

Figure 8 (left) shows the PDF of the fluid vorticity computed at particle positions for different number of particles N_p . We can observe that when the number of particles increases, the variance increases. For $N_p \geq 1.07 \times 10^9/4$, the PDFs of the vorticity computed at the particle position and on the Eulerian grid are almost perfectly superimposed. Figure 8 (right) shows the value of the variance of the fluid vorticity as function of the number of particles. We can observe that the variance increases with the number of particles and reaches the same value as the DNS data for $N_p = 1.07 \times 10^9$.

For fluid particles, the Pearson correlation between the vorticity of the DNS data and the vorticity computed at particle position is $r = 0.93$ for $N_p = 1.5 \times 10^7$ (first data set) and $r = 0.98$ for $N_p = 1.07 \times 10^9$ (second data set). The fact that the correlation is superior to the one obtained in figure 6 (right) is due to the fact that the turbulence has coherent structures while the synthetic velocity field tested in figure 6 (right), although having a similar power spectrum, has no structure.

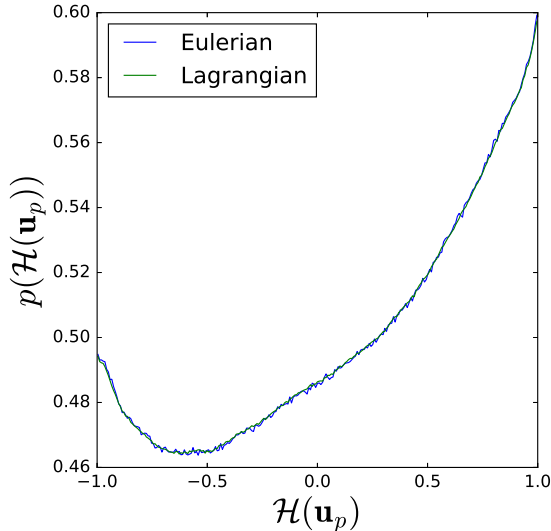


Figure 9. PDFs of the relative helicity (cosine of the angle between particle velocity and vorticity) $\mathcal{H}(\mathbf{u}_p)$ of the particle velocity computed for fluid particles (Lagrangian) and on an Eulerian grid.

The relative helicity of the particle velocity is defined as :

$$\mathcal{H}(\mathbf{u}_p) = \frac{\mathbf{u}_p \cdot \mathcal{C}(\mathbf{u}_p)}{\|\mathbf{u}_p\|_2 \|\mathcal{C}(\mathbf{u}_p)\|_2} \quad (24)$$

This cosine of the angle between the particle velocity and its curl characterizes their alignment. Values of +1 correspond to alignment of both quantities, -1 to anti-alignment and 0 to two-dimensional motion, where the curl is perpendicular to the velocity. Helicity is typically used to quantify swirling motion and coherent vortices, see e.g. [10]. Figure 9 shows the PDF of the relative helicity of the particle velocity for the second data set. We can observe that the value of the helicity computed on the Eulerian grid and at particle positions is perfectly superimposed.

V. CONCLUSIONS

We proposed tessellation-based methods to determine first order differential operators of the particle velocity advecting particle clouds. We analyzed the finite-time measure to quantify the divergence of the particle velocity, proposed in Oujia *et al.* [12]. The underlying idea is to compute the time change of the volume change rate of the Voronoi volume. We proposed a modification of the Voronoi tessellation, i.e., by using the centers of gravity of the Delaunay cells as the vertices of the modified Voronoi cells. We showed that the

modified method converges with first order in time and in each space direction for randomly distributed particles. We showed that the method originally developed to compute the divergence of the particle velocity can be likewise used to compute the curl and velocity gradient tensor by rearranging the velocity vector coefficients. Moreover, we notice that the method has the ability to compute simultaneously the sum of several first order derivatives. Eventually, we applied the method to fluid particles advected in three-dimensional fully developed turbulence and showed that the method gives accurate results for the computation of vorticity and helicity of the fluid particle velocity.

In West *et al.* [19] we applied the above technique to four-way coupled turbulent channel flow data, laden with inertial particles and analyzed the influence of mass loading and inertia of the particles on their clustering in the different flow layers. We computed the divergence and the curl in the log-layer, the buffer layer and the viscous sub-layer and quantified the flow behavior. we studied particle laden isotropic turbulence investigating divergence and curl of the inertial particle velocity. We found extreme divergence and rotation values reflecting the strong intermittency of the particle motion.

Finally let us mention that this method based on the variation of the particle position at two time instants seems to be a natural approach to study the particle motion of PTV data. In addition, the method to compute the divergence from the time variation of the volume can be used in fields where cells appear naturally as in biology.

ACKNOWLEDGEMENTS

T.O. and K.S. acknowledge funding from the Agence Nationale de la Recherche (ANR), grant ANR-20-CE46-0010-01. K.M acknowledges financial support from JSPS KAKENHI Grant Number JP20K04298. Centre de Calcul Intensif d’Aix-Marseille is acknowledged for granting access to its high performance computing resources. The DNS data analyzed in this project were obtained using the Earth Simulator supercomputer system of JAMSTEC. The authors acknowledge use of computational resources from the Yellowstone cluster awarded by the National Science Foundation to CTR.

-
- [1] BARBER, C. B., DOBKIN, D. & HUHDANPAA, H. 1996 The quickhull algorithm for convex hulls, acm transactions on mathematical software. *ACM Trans. Math. Software (TOMS)* **22** (4), 469–483.
- [2] DEJOAN, A. & MONCHAUX, R. 2013 Preferential concentration and settling of heavy particles in homogeneous turbulence. *Phys. Fluids* **25** (1), 013301.
- [3] DELAUNAY, B. 1934 Sur la sphère vide. *Izv. Akad. Nauk SSSR, Otdelenie Matematicheskii i Estestvennyka Nauk* **7** (793-800), 1–2.
- [4] EBELING, H. & WIEDENMANN, G. 1993 Detecting structure in two dimensions combining voronoi tessellation and percolation. *Physical Review E* **47** (1).
- [5] HUERTA, A., BELYTSCHKO, T., FERNÁNDEZ-MÉNDEZ, S. & RABCZUK, T. 2004 Meshfree methods .
- [6] IJZERMANS, R., REEKS, M., MENEGUZ, E., PICCIOTTO, M. & SOLDATI, A. 2009 Measuring segregation of inertial particles in turbulence by a full Lagrangian approach. *Physical Review E* **80** (1), 015302.
- [7] KIRILLOV, A. A. 2008 *An introduction to Lie groups and Lie algebras*, , vol. 113. Cambridge University Press.
- [8] MATSUDA, K., ONISHI, R., HIRAHARA, M., KUROSE, R., TAKAHASHI, K. & KOMORI, S. 2014 Influence of microscale turbulent droplet clustering on radar cloud observations. *J. Atmos. Sci.* **71** (10), 3569–3582.
- [9] MATSUDA, K., SCHNEIDER, K. & YOSHIMATSU, K. 2021 Scale-dependent statistics of inertial particle distribution in high reynolds number turbulence. *Physical Review Fluids* **6** (6), 064304.
- [10] MOFFATT, H. & TSINOBER, A. 1992 Helicity in laminar and turbulent flow. *Annual review of fluid mechanics* **24** (1), 281–312.
- [11] OBLIGADO, M., TEITELBAUM, T., CARTELLIER, A., MININNI, P. & BOURGOIN, M. 2014 Preferential concentration of heavy particles in turbulence. *J. Turbul.* **15** (5), 293–310.
- [12] OUJIA, T., MATSUDA, K. & SCHNEIDER, K. 2020 Divergence and convergence of inertial particles in high-Reynolds-number turbulence. *Journal of Fluid Mechanics* **905**, A14.
- [13] OUJIA, T., MATSUDA, K. & SCHNEIDER, K. 2022 Extreme divergence and rotation values of the inertial particle velocity in high Reynolds number turbulence using Delaunay tessellation.

In *12th International Symposium on Turbulence and Shear Flow Phenomena (TSFP12)*.

- [14] SOZER, E., BREHM, C. & KIRIS, C. C. 2014 Gradient calculation methods on arbitrary polyhedral unstructured meshes for cell-centered cfd solvers. In *52nd Aerospace Sciences Meeting*, p. 1440.
- [15] SQUIRES, K. D. & EATON, J. K. 1990 Particle response and turbulence modification in isotropic turbulence. *Physics of Fluids A: Fluid Dynamics* **2** (7), 1191–1203.
- [16] SQUIRES, K. D. & EATON, J. K. 1991 Preferential concentration of particles by turbulence. *Physics of Fluids A: Fluid Dynamics* **3** (5), 1169–1178.
- [17] VABISHCHEVICH, P. 2005 Finite-difference approximation of mathematical physics problems on irregular grids. *Computational Methods in Applied Mathematics* **5** (3), 294–330.
- [18] VORONOI, G. 1908 Nouvelles applications des paramètres continus à la théorie des formes quadratiques. premier mémoire. sur quelques propriétés des formes quadratiques positives parfaites. *Journal für die reine und angewandte Mathematik* **1908** (133).
- [19] WEST, J., OUJIA, T., MATSUDA, K., SCHNEIDER, K., JAIN, S. & KAZUKI, M. 2022 Divergence and curl of the inertial particle velocity in a four-way coupled turbulent channel flow. In *Center for Turbulence Research, Proceedings of the Summer Program 2022*.